

NJC

Accepted Manuscript



This is an *Accepted Manuscript*, which has been through the Royal Society of Chemistry peer review process and has been accepted for publication.

Accepted Manuscripts are published online shortly after acceptance, before technical editing, formatting and proof reading. Using this free service, authors can make their results available to the community, in citable form, before we publish the edited article. We will replace this *Accepted Manuscript* with the edited and formatted *Advance Article* as soon as it is available.

You can find more information about *Accepted Manuscripts* in the [Information for Authors](#).

Please note that technical editing may introduce minor changes to the text and/or graphics, which may alter content. The journal's standard [Terms & Conditions](#) and the [Ethical guidelines](#) still apply. In no event shall the Royal Society of Chemistry be held responsible for any errors or omissions in this *Accepted Manuscript* or any consequences arising from the use of any information it contains.

Selective Construction of Junctions on Different Facets of BiVO₄ for Enhancing Photo-activity

Peng Wang^{a,b}, Jinyou Zheng^a, Dun Zhang^b and Young Soo Kang^{a*}

^a Korea Center for Artificial Photosynthesis and Department of Chemistry, Sogang University, Seoul 121-742, Korea

^b Key Laboratory of Marine Environmental Corrosion and Bio-fouling, Institute of Oceanology, Chinese Academy of Sciences, 7 Naihai Road, Qingdao 266071, China

*Corresponding Author.

Email address : [yskang@sogang.ac.kr](mailto:ykang@sogang.ac.kr) (Young Soo Kang).

Abstract:

A novel ternary Ag/BiVO₄/Co₃O₄ hybrid photocatalyst was designed by constructing metal-semiconductor junction and p-n junction on electron-rich {010} facet and hole-rich {110} facets of BiVO₄, respectively. The Ag/BiVO₄/Co₃O₄ hybrid photocatalyst exhibits enhanced photocatalytic activity for Rhodamine B degradation, which is over 8 times that of bare BiVO₄ under simulated solar light. It was proven that the combination of metal-semiconductor junction and p-n junction further promotes the charge transferring across the interface, and results in additional effect of two single junctions for improving photo-activity. This research provides a deep insight about the co-working mechanism between two heterojunctions, and it will propose a new concept for designing highly efficient photo-catalyst system.

Keywords: Bismuth vanadate; Photocatalysis; Cobalt oxide; Dye degradation.

1. Introduction

Water purification is quite important for the human health.[1-3] Over recent decades, numerous effective methods have been widely used for water purification, including chlorination, ozonization, UV radiation and so forth.[4-7] However, these treatments have some disadvantages, such as the production of toxic by-products, transport and storage of chemicals as well as high energy needs.[7] Photocatalysis has been proven to be a promising process for water purification for its advantages such as non-selective, and no need of additional chemicals.[8-11]

Bismuth vanadate (BiVO_4) has been received much attention among visible light-active photo-catalysts.[12-14] BiVO_4 has three main crystal structures, tetragonal zircon, tetragonal scheelite and monoclinic scheelite. The monoclinic scheelite phase of BiVO_4 has a band gap of 2.4 eV and has been demonstrated to exhibit much higher photo-catalytic activity in the visible light than the other two phases.[15] However, the photo-activity of BiVO_4 alone is not very impressive because of the relatively fast recombination of photogenerated electron-hole pairs.[16]

Design and constructing heterojunctions, such as p-n junctions, metal-semiconductor (m-s) junctions and so forth, is an effective way to improve the electron-hole separation.[17] Many researchers have reported the advantages of heterojunctions in enhancing activity of photocatalyst.[17-20] Recently, multi-junctions photocatalyst systems were designed to further improve photocatalytic activity, such as $\text{Ag}/\text{Ag}_3\text{PO}_4/\text{BiPO}_4$,[21] and $\text{Cu}-\text{TiO}_2-\text{Cu}_2\text{O}$ [22] hybrid catalysts. In the present research, band position and fermi level were firstly taken into consideration for selecting interface junction materials, since the matching of band energy between two components is one of the most important conditions for designing efficient junctions.[17] Actually, the distribution of hole and electron over semi-conductor surface under irradiation is an essential factor that should be considered for selecting construction location of junctions. However, junctions were usually constructed over semi-conductor surface randomly without considering the location in the present research. In this case, the construction of junctions can hardly achieve optimal hole-electron separation efficiency, and it is also hard to anticipate the co-working mechanism between different junctions for electron-hole separation.

Recently, it was reported that photo-generated electrons and holes can be spatially separated onto different facets of BiVO_4 . [23] Accordingly, we can

selectively construct suitable junctions on different facets of BiVO_4 for improving photoactivity based on the charge separation among different facets. The semiconductor p–n junction is an effective architecture for the highly efficient charge collection and separation. BiVO_4 is an n type semiconductor, so it is reasonable to design p-n junctions on hole-rich facet of BiVO_4 to facilitate the transfer of hole to p-type semiconductor, and thus avoid the recombination of hole with electron in BiVO_4 . To deposit noble metal nanoparticles on the surface of semiconductor is another effective method to create a space-charge separation region. These metal nanoparticles can act as a sink for photo-induced electrons, thereby facilitating the charge separation and enhancing the photocatalytic activity. For their high activity as sink for photo-induced electrons, metal-semiconductor (m-s) junction can be constructed over electron-rich facet of BiVO_4 to improve its photoactivity. So far, various noble metals such as platinum, aurum, and silver have been deposited on semiconductors to improve the photoactivity. Among them, silver is an attractive one because of its low cost and as well as its effective electron trapping ability.[24]

In this research, silver and cobalt oxide were selectively deposited onto electron-rich facet and hole-rich facet of BiVO_4 crystals, thereby constructing metal-semiconductor junction and p-n junction over BiVO_4 . Rhodamine B degradation was utilized as a probe to evaluate the photo-activity of as-fabricated photocatalysts. It was demonstrated that the photoactivity of BiVO_4 with metal-semiconductor junction and p-n junction selectively constructed on $\{010\}$ and $\{110\}$ facets of BiVO_4 crystals was dramatically enhanced compared with the pure BiVO_4 , and the combination of the two junctions results in additional effect of two single junctions for improving photo-activity. This work will give a deep insight to understand the co-working mechanism of multi-junction in a hybrid photocatalyst system, and it will provide a general concept for constructing highly effective photocatalysts.

2. Experimental Section

2.1 Synthesis of photocatalyst

2.1.1 Synthesis of BiVO_4

BiVO_4 crystal sample was synthesized with a hydrothermal method. In a typical procedure, the precursors $\text{Bi}(\text{NO}_3)_3 \cdot 5\text{H}_2\text{O}$ (50 mmol) and NH_4VO_3 (50 mmol) were dissolved in 10 mL of 4.0 M HNO_3 solution and 10 mL 2.0 M NaOH solution, respectively. These two solutions were mixed slowly to form a yellowish suspension, and the pH value of the solution was then adjusted to be 1.0 with sodium hydroxide under stirring. After stirring for 0.5 h, the suspension was transferred into a teflon-lined stainless steel autoclave with a capacity of 25 mL, and reacted at 150 °C for 12 h. After hydrothermal reaction, the precipitate was washed and centrifuged in de-ionized water for three times, and finally dried overnight at 60 °C.

2.1.2 Facet-selective photo-deposition of silver and/or cobalt oxide

For the facet-selective photo-depositions on BiVO_4 , similar procedures were performed for single silver reductive-deposition, single cobalt oxide oxidative-deposition, and simultaneous silver reductive-deposition and cobalt oxide oxidative-deposition. Typically, 0.1 g BiVO_4 powder was dispersed into 50 mL aqueous solution with calculated amount of metal precursors under stirring. Photo-deposition was performed for 4 h at room temperature, and using a 300 W Xe lamp (Max-302, Asahi Spectra, Japan) as a light source. After photo-deposition, BiVO_4 sample was filtered, repeatedly washed with de-ionized water, and finally dried at 40 °C in vacuum oven for 12 h. For single silver reductive-deposition, a 2 g/L AgNO_3 solution with a volume of 50 mL was used as the precursor solution, and the as-obtained sample after photo-deposition was denoted as $\text{BiVO}_4\text{-Ag}$. The single cobalt oxide oxidative-deposition was performed in a 50 mL solution mixed with 1.456 g/L $\text{Co}(\text{NO}_3)_2$ and 4 g/L NaIO_3 , in which, $\text{Co}(\text{NO}_3)_2$ was used as precursor, and NaIO_3 was used as electron acceptors. The as-obtained sample after single oxidative-deposition was denoted as $\text{BiVO}_4\text{-Co}_3\text{O}_4$. The simultaneous silver reductive-deposition and cobalt oxide oxidative-deposition was performed with two-steps procedure. At first, the single cobalt oxide was deposited onto BiVO_4 in a mixed solution with 1.456 g/L $\text{Co}(\text{NO}_3)_2$ and 4 g/L NaIO_3 . After 4 h of photo-deposition, the BiVO_4 sample was filtered, washed with de-ionized water, and

then transferred into 2 g/L AgNO₃ solution. After photo-deposition of Ag, BiVO₄ sample was filtered, repeatedly washed with de-ionized water, and finally dried at 40 °C in vacuum oven for 12 h. The as-obtained sample after two-septs deposition was denoted as BiVO₄-Ag/Co₃O₄.

2.2 Characterization

X-Ray diffraction (XRD, Rigaku miniFlex-II desktop X-ray diffractometer, Cu-K α radiation with $\lambda = 0.154056$ nm) was used to determine crystallinity and the crystal structure of the as-fabricated BiVO₄ samples. The morphologies of the samples were observed by a scanning electron microscope (SEM, Hitachi Horiba S-4300) operated at 20 kV, and by a transmission electron microscope (TEM, JEOL JEM-2010). The chemical states of Ag and Co on BiVO₄ were determined by an X-ray photoelectron spectroscopy apparatus (PHI Quantera SXM). The energies of all spectra were shifted by correcting the C1s peak to 284.6 eV for energy calibration. The room temperature photoluminescence (PL) of the powder samples was measured with a Hitachi F-7000 fluorescence spectrophotometer, using the 325 nm excitation of a Xenon lamp.

2.3 Dye photodegradation experiment

The photocatalytic efficiencies of all the prepared catalysts were evaluated by photodegrading Rhodamine B (RhB) under simulated sunlight irradiation, which was sourced by a 300-W Xe lamp. In the degradation experiment, 100 mg photocatalyst was suspended in 50 mL of aqueous solution with 10 mg L⁻¹ RhB. Before irradiation, the RhB solution with photocatalyst was stirred in the dark for 30 min to reach an adsorption/desorption equilibrium between the RhB and the photocatalyst. During the irradiation, approximately 3-mL suspensions were collected at given time intervals and centrifuged to remove the photocatalyst particles. After that, the absorption spectra of the remaining sample solutions were recorded on the UV-vis equipment. Photocatalytic degradation over each sample was evaluated by the temporal concentration of RhB, which was determined in terms of their standard concentration versus absorbance curves and the changes in intensity of the absorbance

at the corresponding absorption band maximum of RhB (554 nm).

3. Results and discussion

3.1 Morphology and composition characterization

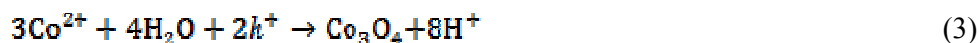
X-Ray diffraction was used to determine crystallinity and the crystal structure of the as-fabricated BiVO₄ samples. According to the X-ray diffraction patterns of as-prepared BiVO₄ powder (Figure 1), It is indicated that the as-prepared BiVO₄ is a monoclinic scheelite according to the standard JCPDS Card of No. 14-0688.

Figure 2 shows the morphologies of bare BiVO₄ powder and BiVO₄ powder deposited with Ag and Co₃O₄ particles. It can be observed that the exposed facets of BiVO₄ are mainly composed of two facets, which are denoted as {010} and {110} facets, respectively (Figure 2a). After photo-reduction deposition in silver nitrate aqueous solution, Ag particles with diameters of around tens of nanometers were selectively deposited on the electron-rich {010} facets of BiVO₄ (Figure 2b). XPS was utilized to confirm the oxidation state of these Ag particles on BiVO₄. From Figure 4a, Ag 3d peaks can be easily observed from the survey spectrum of sample BiVO₄-Ag. The high resolution of Ag 3d spectrum (Figure 4b) shows that two peaks appeared at 368.2 and 374.2 eV are well corresponded with Ag 3d_{5/2} and Ag 3d_{3/2} binding energies, respectively. The splitting of the 3d doublet is 6.1 eV, indicating the metallic nature of silver.[25] Thus, it is proven that the photo-generated electrons are spatially separated onto the {010} facets of BiVO₄ under irradiation, and they are readily available for the reduction reaction of silver ions. It is expected that the photo-reduction of silver ions (equation 1) on {010} facets of BiVO₄ is accompanied by the elimination of photo-generated holes on {110} facets by water oxidation (equation 2), which can be expressed as follows:



Figures 2c and d show the morphologies of BiVO₄ powder after deposition of Co₃O₄ particles with photo-oxidization deposition method in aqueous solution mixed with Co(NO₃)₂ and NaIO₃. As we expect, Co₃O₄ particles are selectively deposited on

the {110} facets of BiVO₄. TEM images (Figures 3a, b) confirm that Co₃O₄ particle layer with thickness of about 20 nm was formed on the {110} facets of BiVO₄ after photo-oxidation deposition. Figure 3c shows the compositional scan profile (blue line marked in the TEM image in Figure 3b on the sample BiVO₄-Co₃O₄. It clearly shows a strong Co signal at the edge of powder, further proving the selective deposition of Co species on {110} facets of BiVO₄. The high resolution of Co 2p XPS spectrum of sample BiVO₄-Co₃O₄ shows a doublet containing a low energy band (Co 2p_{3/2}) and a high energy band (Co 2p_{1/2}) at 780.8 and 796.7 eV (Figure 4c), respectively, indicating that the deposited cobalt species can be ascribed to Co₃O₄.^[26] Accordingly, it is expected that Co²⁺ ions are oxidized into Co₃O₄ on the {110} facets of BiVO₄ crystals with the assistant of using IO₃⁻ as sacrificial electron acceptors. The reactions can be described as equations (3) and (4):



After the selective photo-deposition of Ag and Co₃O₄ particles on BiVO₄, we further investigated the photo-deposition of dual components (Ag and Co₃O₄) with two-step procedure including photo-oxidation deposition and the following photo-reduction deposition. With this method, Ag and Co₃O₄ particles were deposited separately on the {010} and {110} facets of BiVO₄ powder, respectively (Figures 2e and f). XPS was utilized to check the oxidation state of silver and cobalt on BiVO₄ crystals after dual components deposition. It was observed that two typical Ag 3d peaks (Ag 3d_{5/2} and Ag 3d_{3/2}) of BiVO₄-Ag/Co₃O₄ located at the same position with that of BiVO₄-Ag sample (Figure 4b), and the two typical Co 2p peaks (Co2p_{1/2} and Co2p_{3/2}) of BiVO₄-Ag/Co₃O₄ sample also located at the same position with that of BiVO₄-Co₃O₄ sample (Figure 4c). It was demonstrated that the selective deposition of Ag and Co₃O₄ on two facets was successfully accomplished by the two-steps photo-deposition procedure. Thus, the p-n junction and m-s junction can be selectively constructed on hole and electron rich facets of BiVO₄. XPS is generally utilized to determine the content of single composition in the composite material.

According to the XPS result in Figure 4, the content of Ag and Co_3O_4 loaded over BiVO_4 can be calculated as 2.026 wt.% and 0.137 wt.%, respectively.

3.2 Optical absorption property

Diffuse reflectance spectroscopy is an appropriate tool to depict the energy band structure feature of a semiconductor, which is relevant to the optical absorption property considered as a pivotal factor in determining its photocatalytic activity. Figure 5a shows the UV–vis diffuse reflectance spectra of the four kinds of BiVO_4 samples (BiVO_4 , $\text{BiVO}_4\text{-Ag}$, $\text{BiVO}_4\text{-Co}_3\text{O}_4$, and $\text{BiVO}_4\text{-Ag/Co}_3\text{O}_4$). The pure BiVO_4 sample presents intense absorption in the visible region until ~ 525 nm in addition to that in the UV light region.[27, 28] For the monoclinic scheelite BiVO_4 , the visible absorption band is designated to the transition from a valence band formed by Bi_{6s} or a hybrid orbital of Bi_{6s} and O_{2p} to a conduction band of V_{3d} .[28] The band gap (E_g) of the sample can be estimated according to formula $ah\nu = A(h\nu - E_g)^{n/2}$, [28] where a , h , ν , A and E_g are the absorption coefficient, Planck's constant, the incident light frequency, a constant and the band gap energy, respectively. For BiVO_4 , the value of n is 1, which indicates that BiVO_4 is a direct band gap material. From the plots of $(ah\nu)^2$ versus photon energy ($h\nu$) shown in Figure 5b, the band gap energy of BiVO_4 could be estimated as 2.43 eV.[29]

After the deposition of Co_3O_4 , the ability of light absorption is enhanced greatly. In accordance with that, the color of sample changed from yellow of pure BiVO_4 to grey-yellow of $\text{BiVO}_4\text{-Co}_3\text{O}_4$ (Figure 5c). This should be attributed to the broad absorption at 500–900 nm characteristic of the Co_3O_4 phase.[30] After the deposition of Ag, the absorbance edge of $\text{BiVO}_4\text{-Ag}$ shows a slight red shift, and the absorption of BiVO_4 in the range of 500–800 nm is intensified, both of it can be attributed to the surface plasmon resonance effect of silver nanoparticles.[31] After the deposition of two components (Ag and Co_3O_4), the absorption of BiVO_4 in the range of 500–800 nm is further enhanced in comparison with BiVO_4 samples deposited with single Ag or single Co_3O_4 component, and this result agrees with the phenomenon that the color of sample $\text{BiVO}_4\text{-Ag/Co}_3\text{O}_4$ is darker than samples $\text{BiVO}_4\text{-Ag}$ and $\text{BiVO}_4\text{-Co}_3\text{O}_4$. It must be emphasized that the photocatalytic activity can be greatly increased when the

band gap is narrowed, which can facilitate the generation of electrons and holes and the excitation of an electron from the valence band to the conduction band.[32] The estimated E_g of as-fabricated $\text{BiVO}_4\text{-Co}_3\text{O}_4$, $\text{BiVO}_4\text{-Ag}$ and $\text{BiVO}_4\text{-Ag/Co}_3\text{O}_4$ from the intercept of the slopes to the plots were 2.41, 2.40 eV and 2.37 eV, respectively. The band gaps of these samples decreased compared to pure BiVO_4 (2.43 eV), and the lower band gap implies a higher photocatalytic activity in the visible light under irradiation for the presence of Ag and Co_3O_4 .

3.3 Photocatalytic activity and mechanism

To prove the contribution of Ag and Co_3O_4 to the photocatalytic activities of BiVO_4 , and to understand the co-working mechanism of multi-junction in a hybrid photocatalyst system, the photocatalytic activities of samples BiVO_4 , $\text{BiVO}_4\text{-Ag}$, $\text{BiVO}_4\text{-Co}_3\text{O}_4$, and $\text{BiVO}_4\text{-Ag/Co}_3\text{O}_4$ were firstly measured in the liquid phase reaction under the simulated solar light irradiation. The decomposition of RhB in the aqueous solution was chosen as the photoreaction probe. As shown in Figure 6, the adsorption of RhB over all samples in dark condition could be neglected. After 120 min of the simulated solar light irradiation, degradation extent of RhB dye with the assistant of pure BiVO_4 can only reach around 10%, indicating that BiVO_4 only achieves low activity for degradation of RhB. In the presence of BiVO_4 powders deposited with single component (Ag or Co_3O_4), the degradation extents of RhB dye increase to 20% (sample $\text{BiVO}_4\text{-Co}_3\text{O}_4$) and 52% (sample $\text{BiVO}_4\text{-Ag}$), respectively. It indicates that the single Ag or Co_3O_4 component on BiVO_4 powder can increase photocatalytic activities. In the presence of sample $\text{BiVO}_4\text{-Ag/Co}_3\text{O}_4$, the degradation extent of RhB is further increased to 65%, proving that a better performance can be achieved by depositing the two components simultaneously.

If the photo-degradation of RhB is considered as a pseudo-first-order reaction, its photocatalytic reaction kinetics can be expressed as follows: $\ln(C/C_0) = kt$, where C is the concentration of the RhB at time t , C_0 is the initial concentration of the RhB solution, and the slope k is the apparent reaction rate constant. Figure 6b represents the photodegradation curves of RhB in the form of $\ln(C_0/C)$ as a function of irradiation time. It can be found that the apparent reaction rate constant of sample

BiVO₄ for RhB photo-degradation is $9.87 \times 10^{-4} \text{ min}^{-1}$. After depositing the two components (Ag and Co₃O₄) simultaneously, the apparent reaction rate constant of sample BiVO₄-Ag/Co₃O₄ for RhB photo-degradation increases to $81.5 \times 10^{-4} \text{ min}^{-1}$, which is almost ten times that of bare BiVO₄. It is proven that the deposition of the two components can significantly improve the photoactivity of photocatalyst. It should be noticed that the apparent reaction rate constant of sample BiVO₄-Ag/Co₃O₄ is almost equal to the sum of that of samples BiVO₄-Ag and BiVO₄-Co₃O₄ ($k_{\text{BiVO}_4\text{-Ag/Co}_3\text{O}_4} \approx k_{\text{BiVO}_4\text{-Ag}} + k_{\text{BiVO}_4\text{-Co}_3\text{O}_4}$), indicating that there is no synergetic effect between the p-n junction and metal-semiconductor junction in the Co₃O₄/BiVO₄/Ag system.

PL emission spectra are often used to examine the efficiency of charge carrier trapping, immigration and transfer, as well as understand the fate of electron/hole pairs in semiconductor particles. Figure 7 shows the room temperature PL emission spectra of samples BiVO₄, BiVO₄-Co₃O₄, BiVO₄-Ag, BiVO₄-Ag/Co₃O₄. The PL peak of as-fabricated BiVO₄ powder was observed at around 540 nm, and it corresponds to the recombination of the hole formed in the O_{2p} band and the electron in the V_{3d} band. In comparison with bare BiVO₄, the PL peak is reduced after depositing single Co₃O₄ or single Ag component, indicating that the existence of the single component can help to reduce the recombination of electron and hole. The PL peak of the sample BiVO₄-Ag/Co₃O₄ is further reduced after depositing Ag and Co₃O₄ simultaneously. This result indicates that the recombination of photogenerated charge carrier is greatly inhibited, and photo-activity of photocatalyst will be enhanced greatly after depositing Ag and Co₃O₄ simultaneously.

Based on these results, the charge separation process of Co₃O₄/BiVO₄/Ag heterogeneous structures can be proposed as Figure 8. The band gap of BiVO₄ was evaluated as 2.43 eV from the UV-vis spectrum. Therefore we presume the corresponding conduction band (E_{CB}) and valence band (E_{VB}) positions of BiVO₄ at the point of zero charge through the following equations [33]:

$$E_{\text{CB}} = x - E_0 - \frac{1}{2}E_g \quad (5)$$

$$x = \frac{1}{2}(A_f + I_1) \quad (6)$$

where x is the bulk electronegativity of the compound, A_f and I_1 are the atomic electron affinity and the first ionization potential, respectively. E_0 is the energy of free electrons on the hydrogen scale (about 4.5 eV), and E_g is the band gap energy of the semiconductor. The position of the valence band edge can be determined by the equation of $E_{\text{VB}} = E_{\text{CB}} + E_g$. The calculation result shows that the bottom of the conduction band of BiVO_4 is around 0.32 eV versus normal hydrogen electrode (NHE), while the top of the valence band is around 2.75 eV. Generally speaking, the conduction band potential of n-type semiconductor is more negative (ca. 0.1 – 0.2 V) than the flat-band potentials,[33] so the Fermi level of metallic Ag ($E_f = 0.69$ V vs. NHE) is much lower than that of BiVO_4 . [34] On the {010} facet of BiVO_4 , when Ag and BiVO_4 are in contact, electrons in BiVO_4 will transfer to the Ag particles to equilibrate the Fermi levels, and a Schottky barrier forms between Ag and BiVO_4 . Furthermore, it was widely reported that Co_3O_4 is a kind of p-type semi-conductor with conduction band edge and valence band edge of Co_3O_4 of 0.37 eV and 2.44 eV vs. NHE. Before contact of p-type Co_3O_4 with n-type BiVO_4 , the conduction band edge of p-type Co_3O_4 is lower than that of n-type BiVO_4 , and the Fermi level of the Co_3O_4 is also lower than that of the BiVO_4 , as shown in Figure 8a. After the p-type Co_3O_4 nanoparticles are tightly assembled on the hole-rich facet {110} of n-type BiVO_4 nanocrystals, the Fermi level of Co_3O_4 is raised up, while the Fermi level of BiVO_4 is lowered until an equilibrium state is formed as shown in Figure 8b. Meanwhile, with the raising up and/or lowering of the Fermi level, the whole energy band of Co_3O_4 is raised up while that of BiVO_4 is lowered down, and as a result, the conduction band edge of p-type Co_3O_4 is higher than that of n-type BiVO_4 , leading to

the formation of a p–n junction at the interface between Co_3O_4 and BiVO_4 crystals.

In the $\text{Ag}/\text{BiVO}_4/\text{Co}_3\text{O}_4$ system, the electrons and holes transfer separately to $\{010\}$ and $\{110\}$ facets of BiVO_4 for the potential difference between the two facets under irradiation. On the electron-rich $\{010\}$ facet, electron can be easily injected into the Fermi level of Ag. The metallic silver nanoparticles functioned as an electron sink to accept the photo-generated electrons from the excited semiconductor, thereby facilitating dioxygen reduction.[35] On the hole-rich $\{110\}$ facet, the photo-generated holes on the valence band of n-type BiVO_4 can be promptly migrated to the valence band of p-type Co_3O_4 , and the photo-generated electrons on the conduction band of p-type Co_3O_4 can be transferred to the conduction band of n-type BiVO_4 . Such a migration of photo-generated carriers can be promoted by the internally formed electric field. Therefore, the photo-generated electrons and holes of n-type BiVO_4 can be separated effectively by the p–n junctions formed between the p-type Co_3O_4 and n-type BiVO_4 interface, and the recombination of electron–hole pairs can be substantially reduced. As a result, $\text{Ag}/\text{BiVO}_4/\text{Co}_3\text{O}_4$ had a quicker charge separation and slower charge recombination process than single or two components catalyst system. The combination of the two junctions in the $\text{Ag}/\text{BiVO}_4/\text{Co}_3\text{O}_4$ system results in additional effect for improving photo-activity.

4. Conclusion

A novel ternary $\text{Ag}/\text{BiVO}_4/\text{Co}_3\text{O}_4$ hybrid photocatalyst was designed with photo-deposition method. In this hybrid photocatalyst, metal-semiconductor junction and p-n junction were separately constructed over $\{010\}$ facet and $\{110\}$ facet of BiVO_4 , which are electron-rich and hole-rich facets, respectively. The $\text{Ag}/\text{BiVO}_4/\text{Co}_3\text{O}_4$ system exhibits enhanced photocatalytic activity for Rhodamine B degradation, which is over 8 times that of bare BiVO_4 under irradiation. The apparent reaction rate constant of sample $\text{BiVO}_4\text{-Ag}/\text{Co}_3\text{O}_4$ is almost equal to the sum of that of samples $\text{BiVO}_4\text{-Ag}$ and $\text{BiVO}_4\text{-Co}_3\text{O}_4$. It is proven that the combination of the two junctions further promotes the charge transferring across the interface, and results in an additional effect of the two single junctions for improving photo-activity. This

research provides a deep insight about the co-working mechanism between two heterojunctions, and it will propose a new concept for designing highly efficient photocatalyst system.

Acknowledgement

This research was supported by the Young Scientist Exchange Program between The Republic of Korea and the People's Republic of China, and The National Natural Science Foundation of China (No. 41476068).

References

- 1 J.M.C. Robertson, P.K.J. Robertson, L.A. Lawton, *J. Photoch. Photeobio, A*, 2005, **175**, 51-56.
- 2 H.A. Foster, I.B. Ditta, S. Varghese, A. Steele, *Appl. Microbiol. Biotechnol*, 2011, **90**, 1847-1868.
- 3 X. Wang, X. Hu, H. Wang, C. Hu, *Water Res.*, 2012, **46**, 1225-1232.
- 4 J. Oh, D.E. Salcedo, C.A. Medriano, S. Kim, *J. Environ. Sci.*, 2014, **26**, 1238-1242.
- 5 Y. Mao, X. Wang, H. Yang, H. Wang, Y.F. Xie, *Chemosphere*, 2014, **117**, 515-520.
- 6 C. Poepping, S.E. Beck, H. Wright, K.G. Linden, *Water Res.*, 2014, **56**, 181-189.
- 7 E. Ortega-Gómez, P. Fernández-Ibáñez, M.M. Ballesteros Martín, M.I. Polo-López, B. Esteban García, J.A. Sánchez Pérez, *Water Res.*, 2012, **46**, 6154-6162.
- 8 T. Matsunaga, R. Tomoda, T. Nakajima, H. Wake, *FEMS Microbiol. Lett.*, 1985, **29**, 211-214.
- 9 P. Xiong, J. Hu, *Water Res.*, 2013, **47**, 4547-4555.
- 10 L. Zhang, H. Wang, Z. Chen, P.K. Wong, J. Liu, *Appl. Catal. B Environ.*, 2011, **106**, 1-13.
- 11 J. Cao, B. Luo, H. Lin, S. Chen, *J. Hazard. Mater.*, 2011, **190**, 700-706.
- 12 S.J. Hong, S. Lee, J.S. Jang, J.S. Lee, *Energ. Environ. Sci.*, 2011, **4**, 1781-1787.
- 13 D.K. Zhong, S. Choi, D.R. Gamelin, *J. Am. Chem. Soc.*, 2011, **133**, 18370-18377.
- 14 R. Saito, Y. Miseki, K. Sayama, *Chem. Commun.*, 2012, **48**, 3833-3835.
- 15 H. Fan, T. Jiang, H. Li, D. Wang, L. Wang, J. Zhai, D. He, P. Wang, T. Xie, *J. Phys. Chem. C*, 2012, **116**, 2425-2430.
- 16 S.W. Cao, Z. Yin, J. Barber, F.Y.C. Boey, S.C.J. Loo, C. Xue, *ACS Appl. Mater. Interfaces*, 2012, **4**, 418-423.
- 17 H. Wang, L. Zhang, Z. Chen, J. Hu, S. Li, Z. Wang, J. Liu, X. Wang, *Chem. Soc. Rev.*, 2014, **435**, 234-5244.
- 18 W. Wang, X. Huang, S. Wu, Y. Zhou, L. Wang, H. Shi, Y. Liang, B. Zou, *Appl. Catal. B Environ.*, 2013, **134-135**, 293-301.
- 19 W. Wang, J. Wang, Z. Wang, X. Wei, L. Liu, Q. Ren, W. Gao, Y. Liang, H. Shi, *Dalton Trans.*, 2014, **43**, 6735-6743.
- 20 Z. He, Y. Shi, C. Gao, L. Wen, J. Chen, S. Song, *J. Phys. Chem. C*, 2014, **118**, 389-398.
- 21 Y. Lv, K. Huang, W. Zhang, B. Yang, F. Chi, S. Ran, X. Liu, *Ceram. Int.*, 2014, **40**, 8087-8092.

- 22 X. An, H. Liu, J. Qu, S.J.A. Moniz, J. Tang. *New J. Chem.*, 2015, **39**, 314-320.
- 23 R. Li, F. Zhang, D. Wang, J. Yang, M. Li, J. Zhu, X. Zhou, H. Han, C. Li, *Nat. Commun.*, 2013, **4**, 1432.
- 24 L. Chen, R. Huang, Y.J. Ma, S.L. Luo, C.T. Au, S.F. Yin, *RSC Adv.*, 2013, **3**, 24354-24361
- 25 P. Zhang, C. Shao, Z. Zhang, M. Zhang, J. Mu, Z. Guo, Y. Liu, *Nanoscale*, 2011, **3**, 3357-3363.
- 26 J. Xu, P. Gao, T.S. Zhao, *Energy Environ. Sci.*, 2012, **5**, 5333-5339.
- 27 A. Kudo, I. Tsuji, H. Kato, *Chem. Commun.*, 2002, 1958.
- 28 Y. Lu, Y.S. Luo, H.M. Xiao, S.Y. Fu. *CrystEngComm*, 2014, **16**, 6059-6065.
- 29 Z. He, Y. Shi, C. Gao, L. Wen, J. Chen, S. Song, *J. Phys. Chem. C*, 2014, **118**, 389-398.
- 30 J. Wang, F.E. Osterloh, *J. Mater. Chem. A*, 2014, **2**, 9405-9411
- 31 A.Y. Booshehri, S.C.K. Goh, J. Hong, R. Jiang, R. Xu, *J. Mater. Chem. A*, 2014, **2**, 6209-6217
- 32 Z.Y. Bian, Y.Q. Zhu, J.X. Zhang, A.Z. Ding, H. Wang, *Chemosphere*, 2014, **117**, 527-531.
- 33 Y. Hu, D. Li, Y. Zheng, W. Chen, Y. He, Y. Shao, X. Fu, G. Xiao, *Appl. Catal. B Environ.*, 2011, **104**, 30-36.
- 34 W. Fan, S. Jewell, Y. She, M.K.H. Leung, *Phys. Chem. Chem. Phys.*, 2014, **16**, 676.
- 35 Y. Yang, J. Wen, J. Wei, R. Xiong, J. Shi. C. Pan, *ACS Appl. Mater. Interfaces*, 2013, **5**, 6201-6207.

Figure captions

Figure 1. X-ray diffraction pattern of as-prepared monoclinic sheelite BiVO_4 powder.

Figure 2. Morphologies of as-prepared BiVO_4 powder (a), sample $\text{BiVO}_4\text{-Ag}$ (b), sample $\text{BiVO}_4\text{-Co}_3\text{O}_4$ (c, d) and sample $\text{BiVO}_4\text{-Ag/Co}_3\text{O}_4$ (e, f). Scale bar = 500nm.

Figure 3. TEM images of sample $\text{BiVO}_4\text{-Co}_3\text{O}_4$ (a, b), and the EDS line scan of Bi, V, Co and O elements on sample $\text{BiVO}_4\text{-Co}_3\text{O}_4$ along blue line marked in Figure b (c).

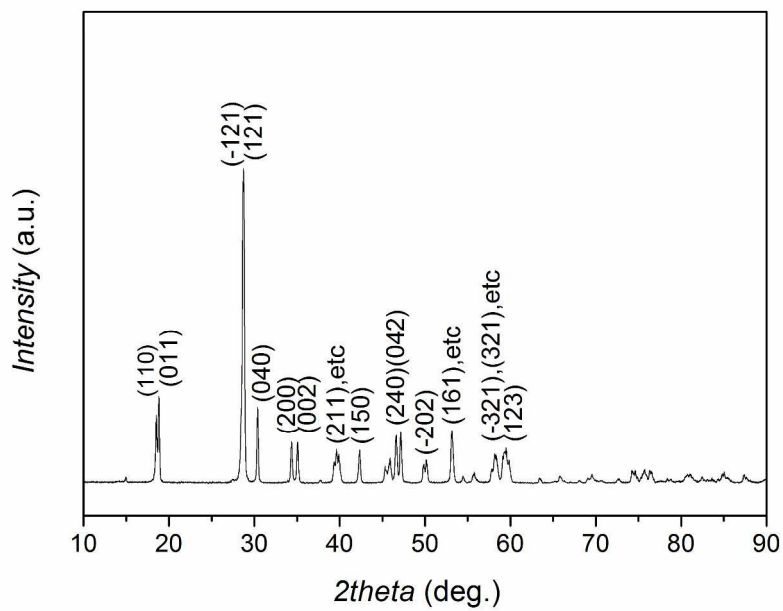
Figure 4. XPS spectra of three kinds of photo-catalyst ($\text{BiVO}_4\text{-Ag}$, $\text{BiVO}_4\text{-Co}_3\text{O}_4$ and $\text{BiVO}_4\text{-Ag/Co}_3\text{O}_4$): (a) Survey spectra, high resolution of (b) Ag 3d and (c) Co 2p spectra.

Figure 5. UV–VIS DRS of samples BiVO_4 , $\text{BiVO}_4\text{-Ag}$, $\text{BiVO}_4\text{-Co}_3\text{O}_4$, and $\text{BiVO}_4\text{-Ag/Co}_3\text{O}_4$ (a), plots of $(\alpha h\nu)^2$ vs. $h\nu$ (b), and photos of samples BiVO_4 , $\text{BiVO}_4\text{-Ag}$, $\text{BiVO}_4\text{-Co}_3\text{O}_4$, and $\text{BiVO}_4\text{-Ag/Co}_3\text{O}_4$ (c).

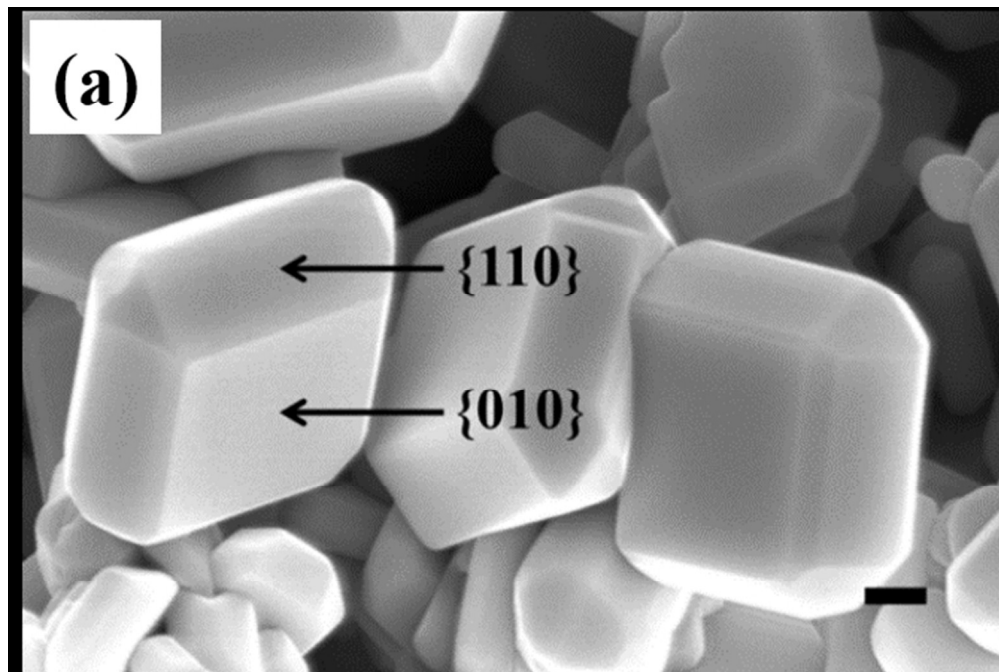
Figure 6. Photo-degradation extent of RhB dye versus irradiation time in the presence of samples BiVO_4 , $\text{BiVO}_4\text{-Co}_3\text{O}_4$, $\text{BiVO}_4\text{-Ag}$, $\text{BiVO}_4\text{-Ag/Co}_3\text{O}_4$ (a), and kinetic curves for the photo-degradation of RhB dye under the irradiation (b).

Figure 7. Room temperature PL emission spectra of samples BiVO_4 , $\text{BiVO}_4\text{-Co}_3\text{O}_4$, $\text{BiVO}_4\text{-Ag}$, $\text{BiVO}_4\text{-Ag/Co}_3\text{O}_4$.

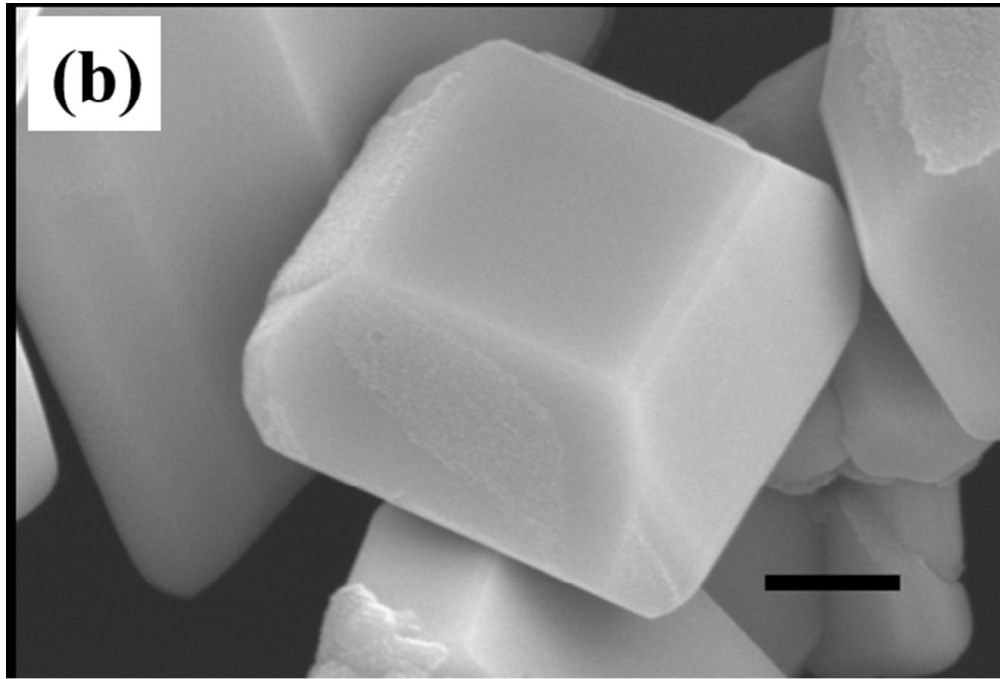
Figure 8. A schematics on the charge transfer processes of $\text{Ag/BiVO}_4\text{/Co}_3\text{O}_4$ hybrid photocatalyst.



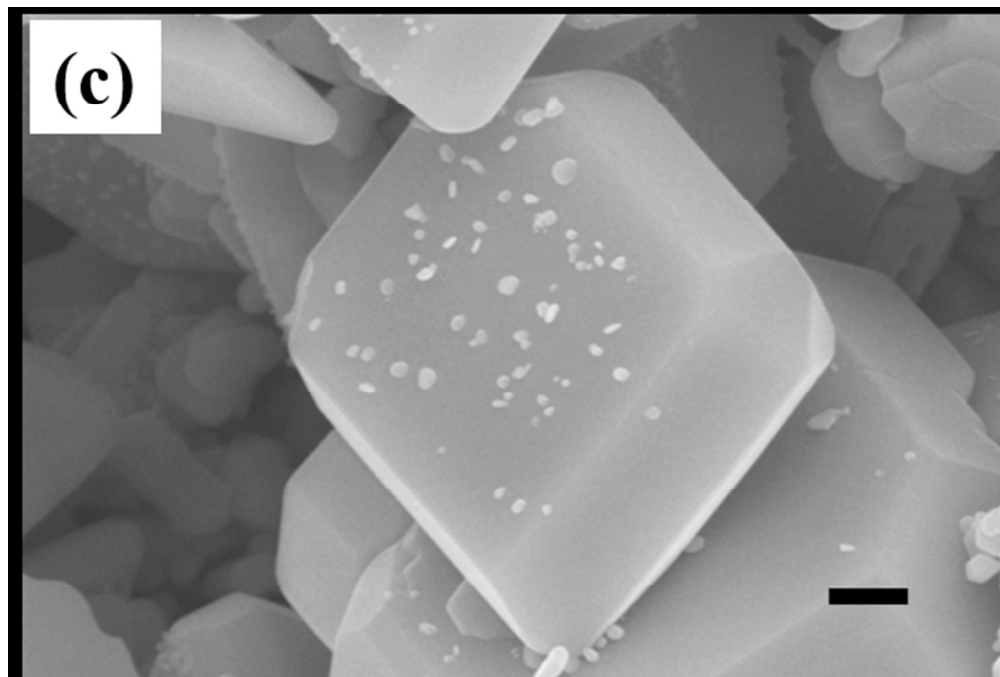
287x201mm (300 x 300 DPI)



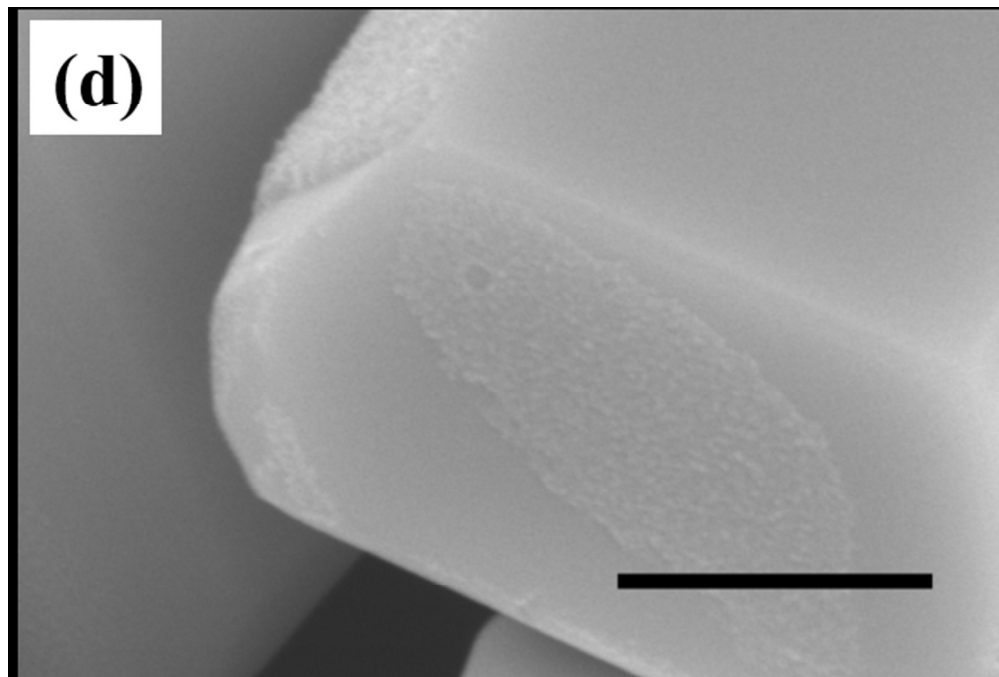
113x75mm (150 x 150 DPI)



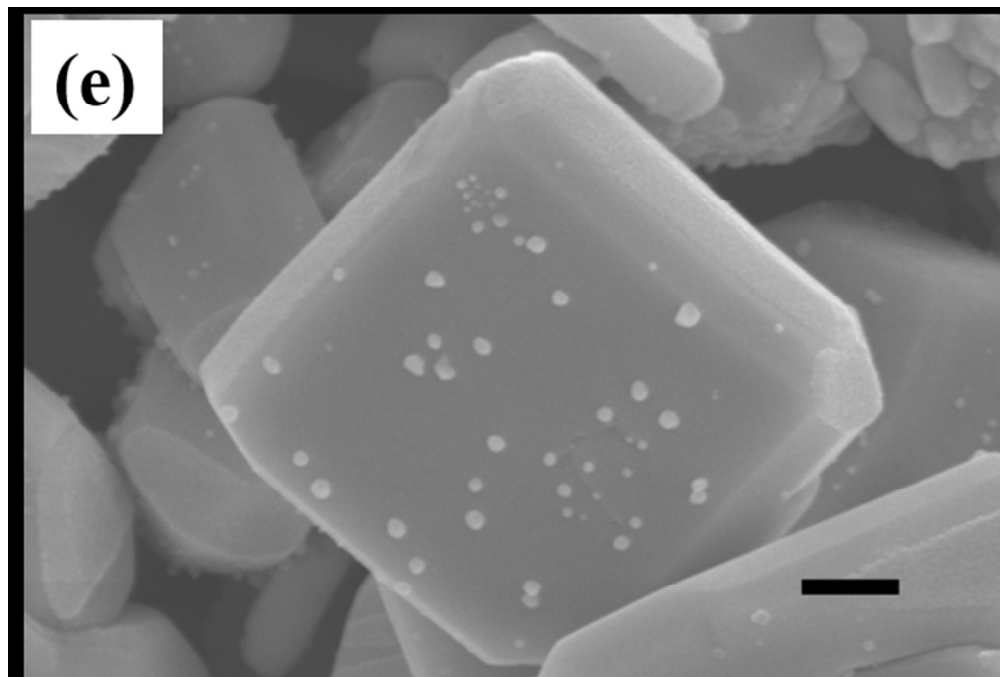
112x75mm (150 x 150 DPI)



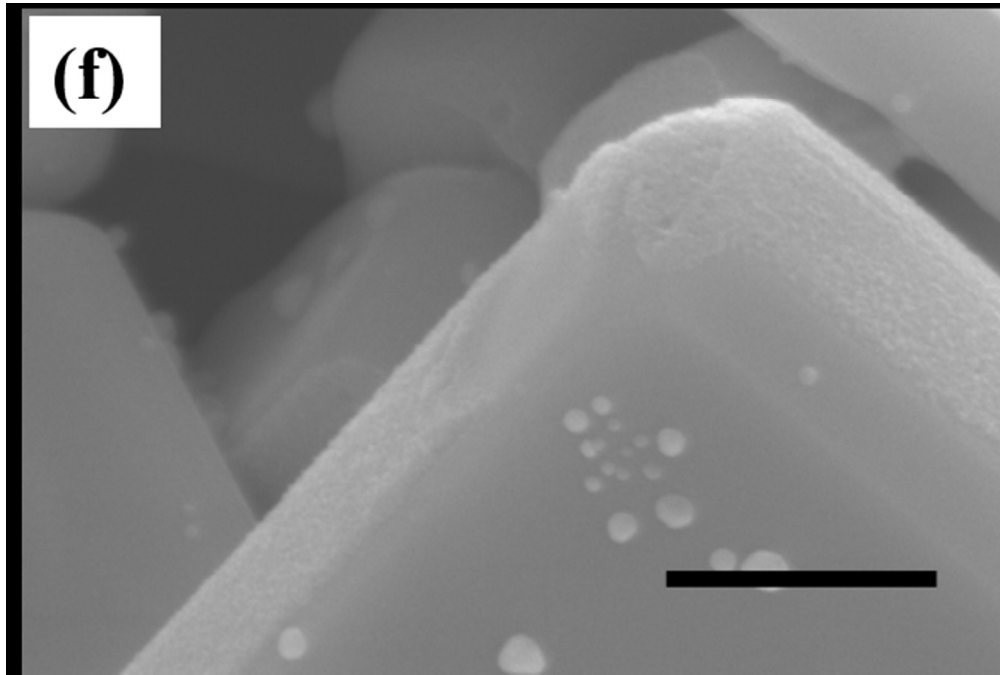
113x76mm (150 x 150 DPI)



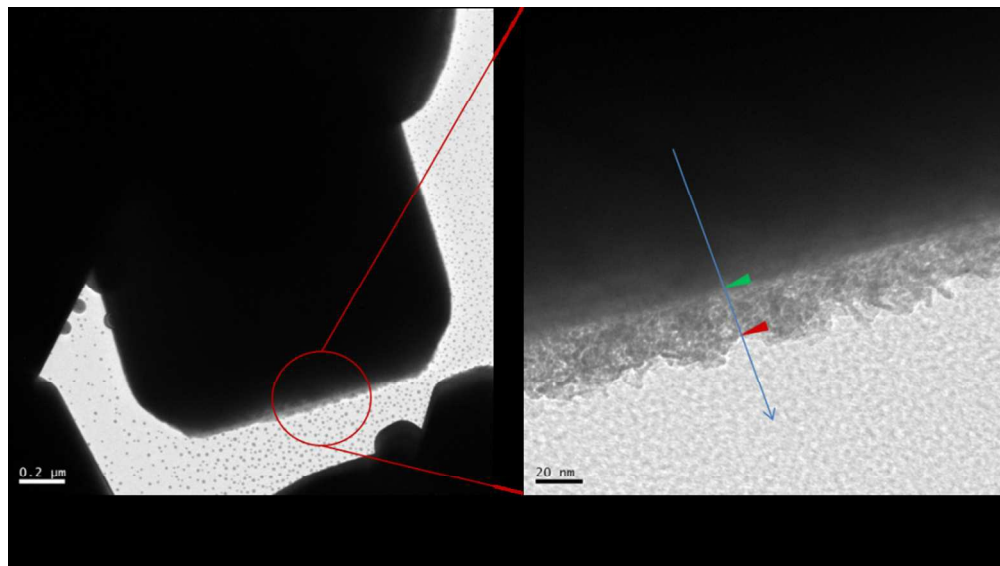
113x76mm (150 x 150 DPI)



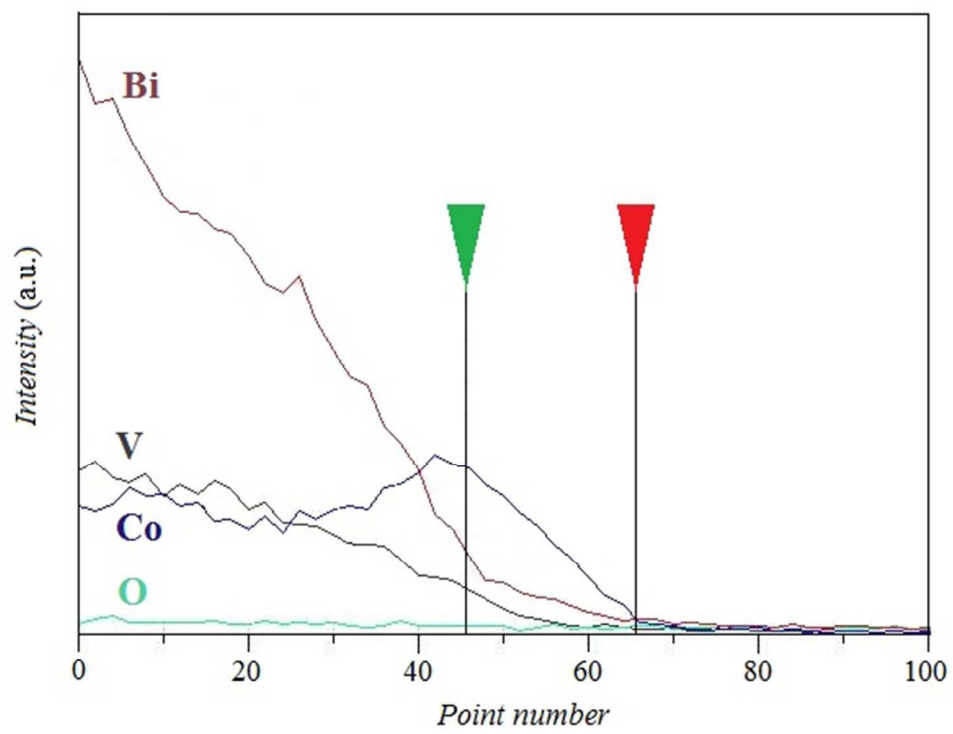
113x76mm (150 x 150 DPI)



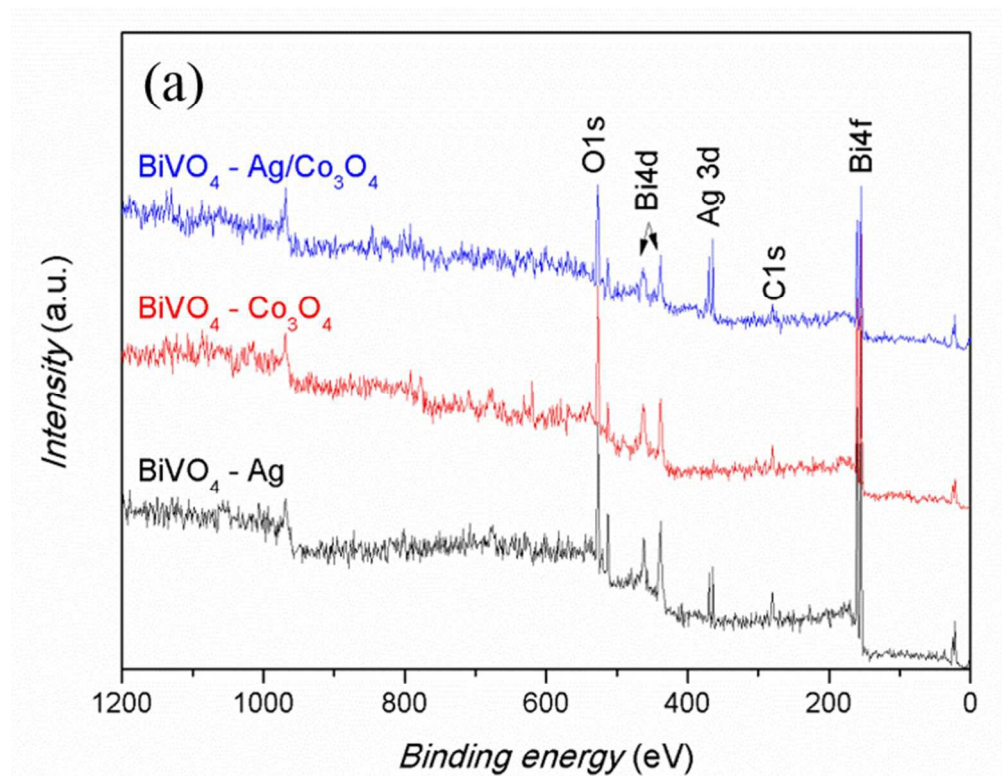
113x76mm (150 x 150 DPI)



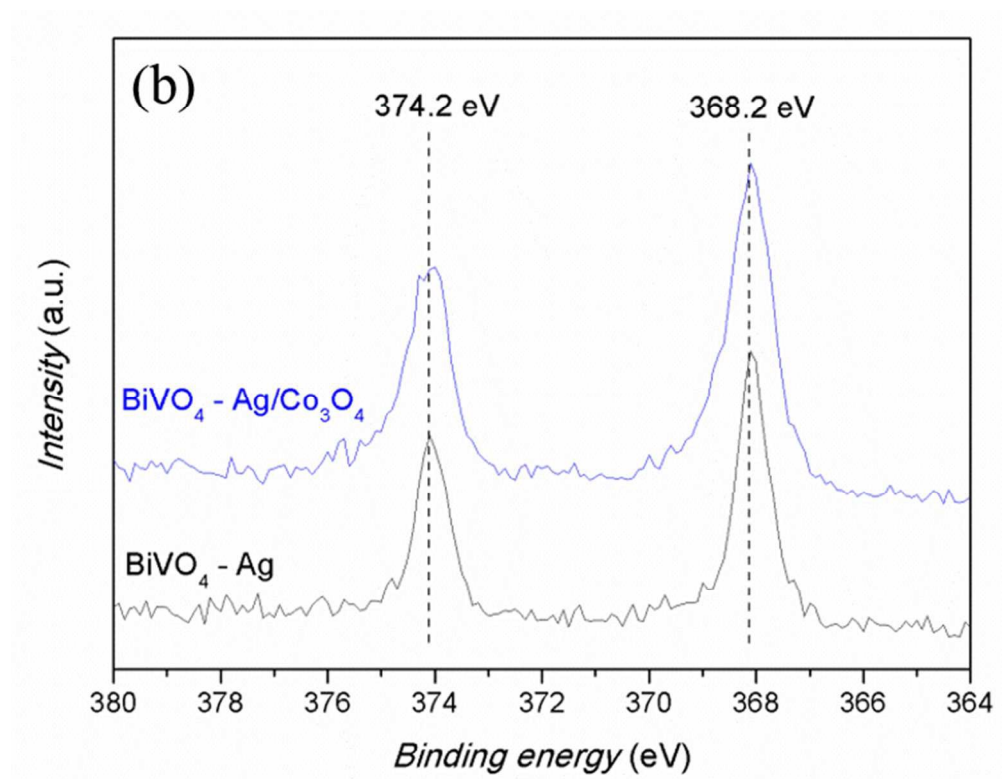
218x123mm (150 x 150 DPI)



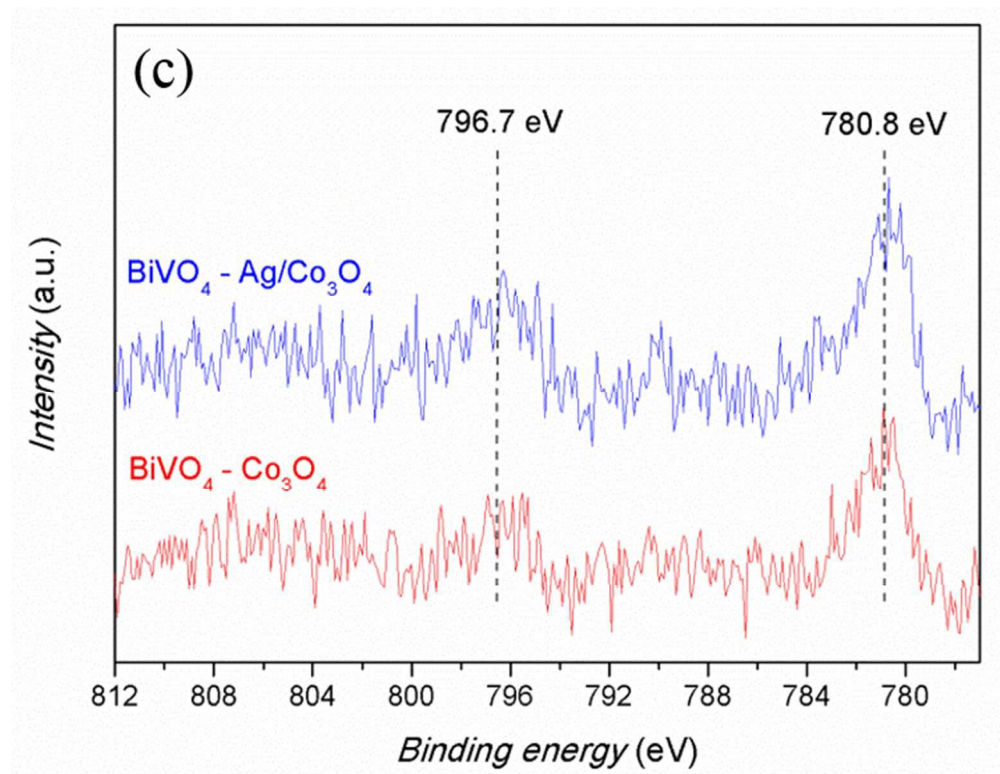
146x127mm (150 x 150 DPI)



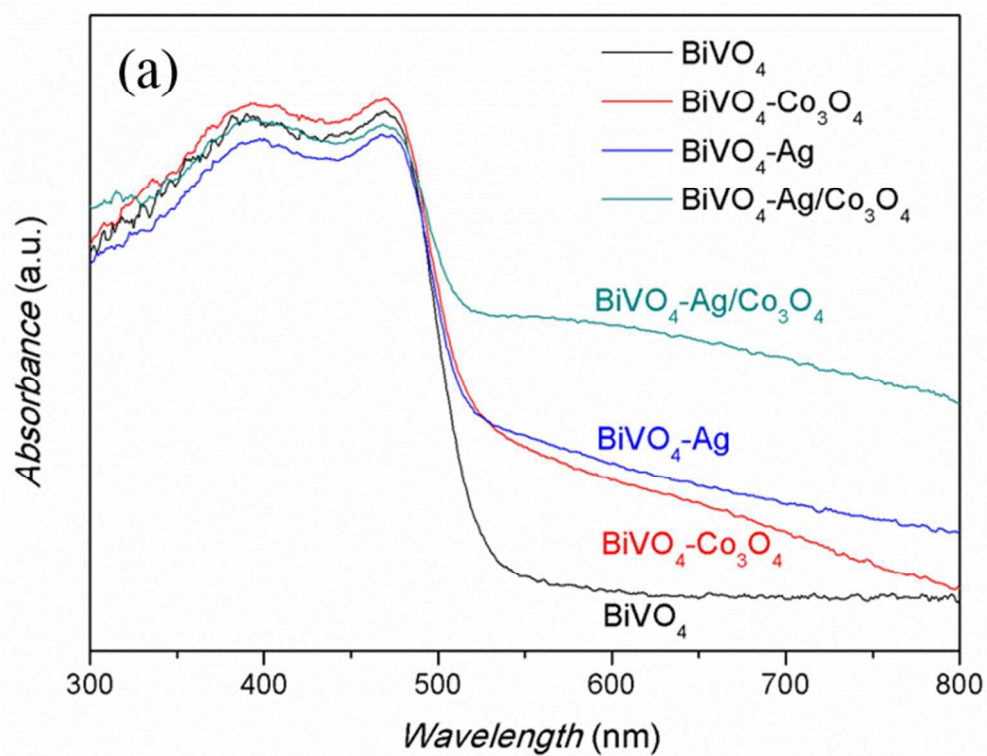
127x98mm (150 x 150 DPI)



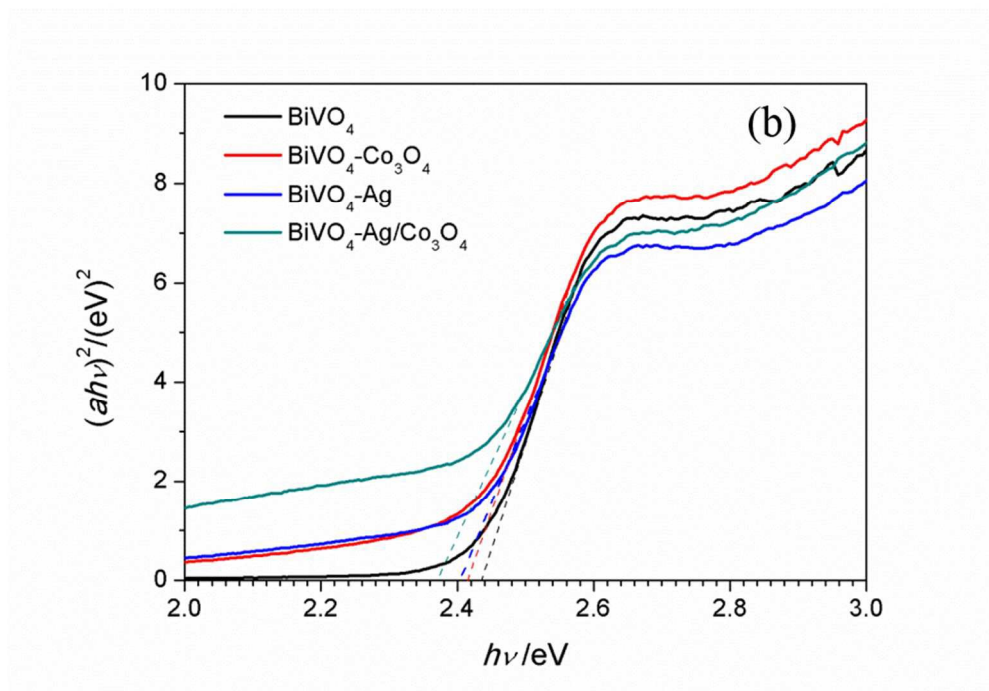
126x98mm (150 x 150 DPI)



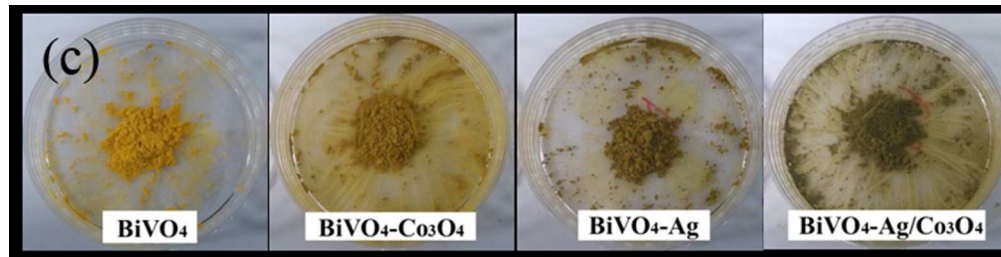
127x98mm (150 x 150 DPI)



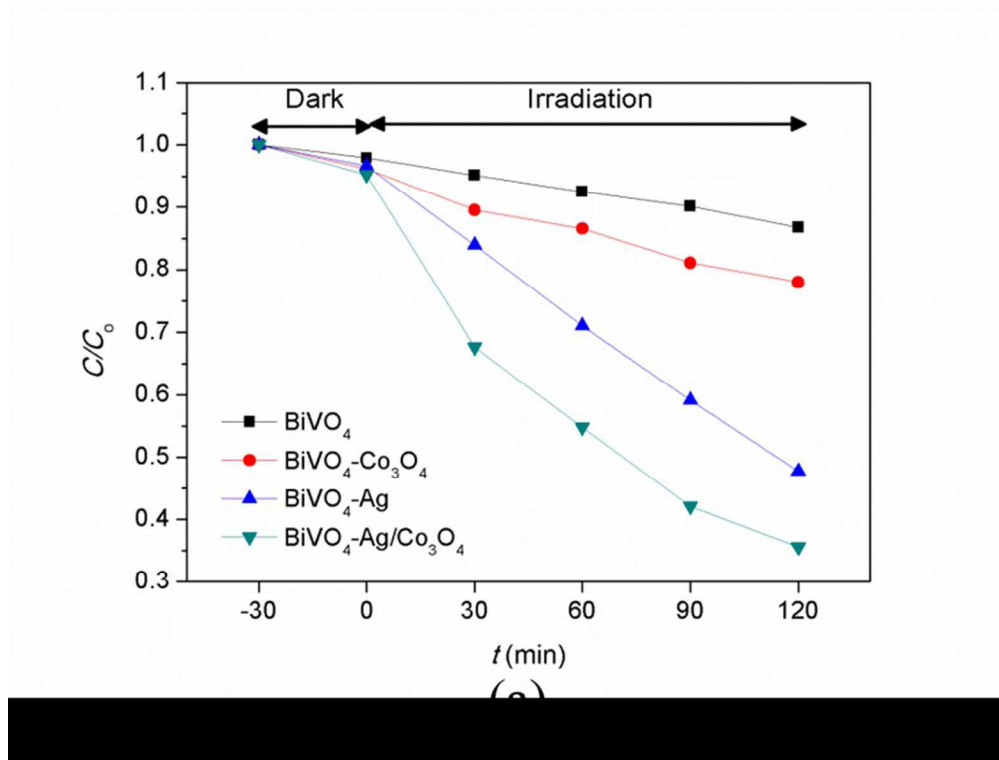
127x97mm (150 x 150 DPI)



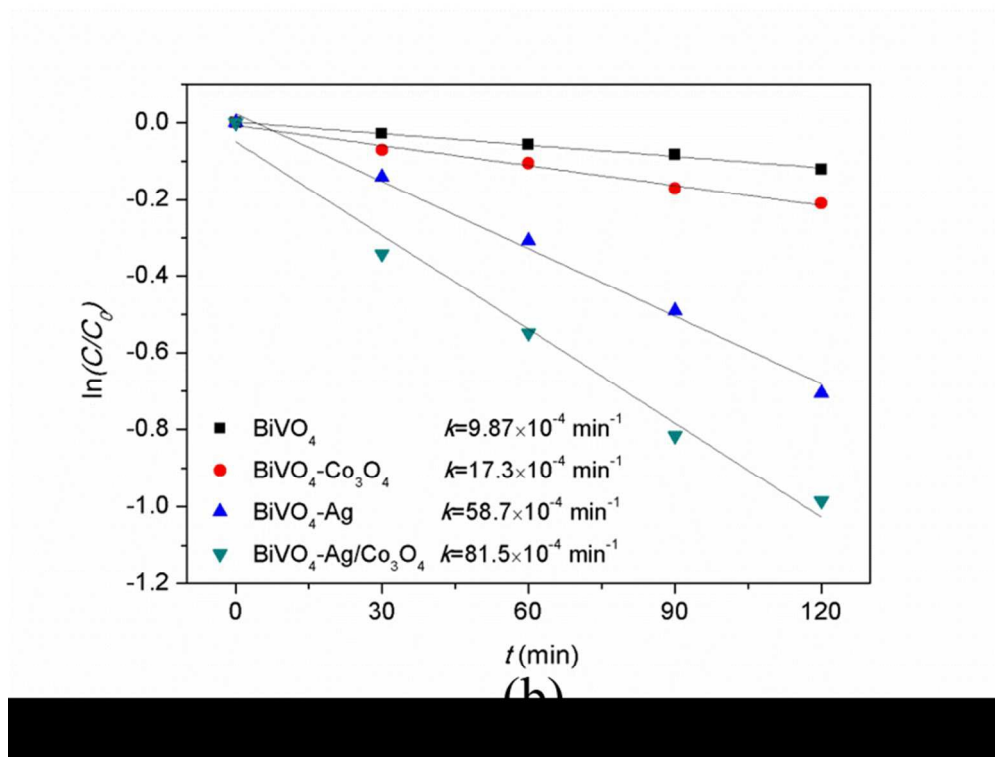
164x113mm (150 x 150 DPI)



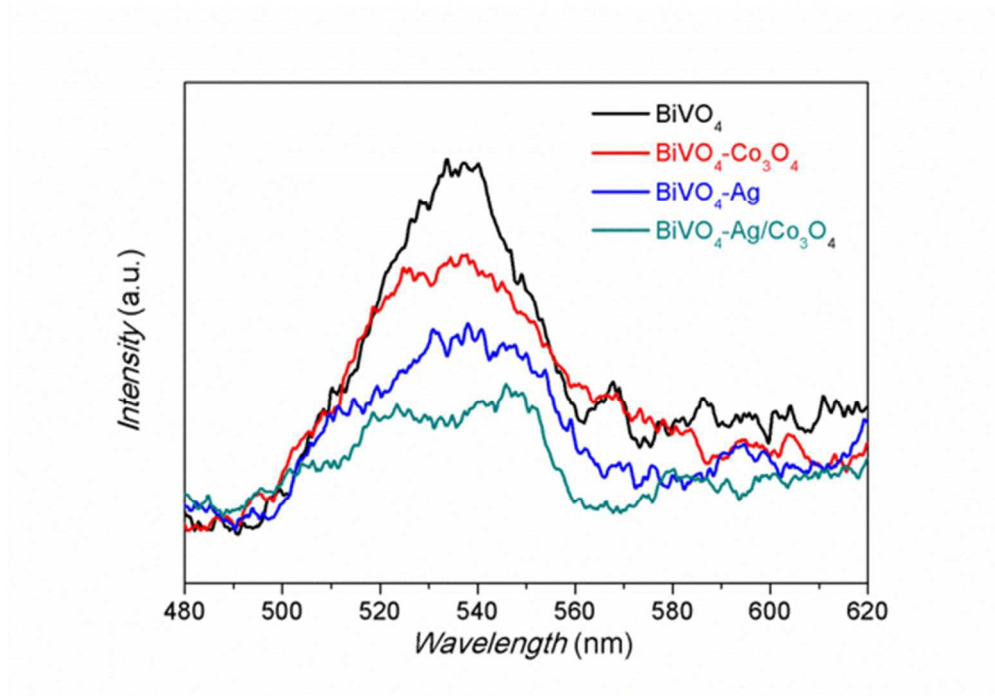
133x33mm (150 x 150 DPI)



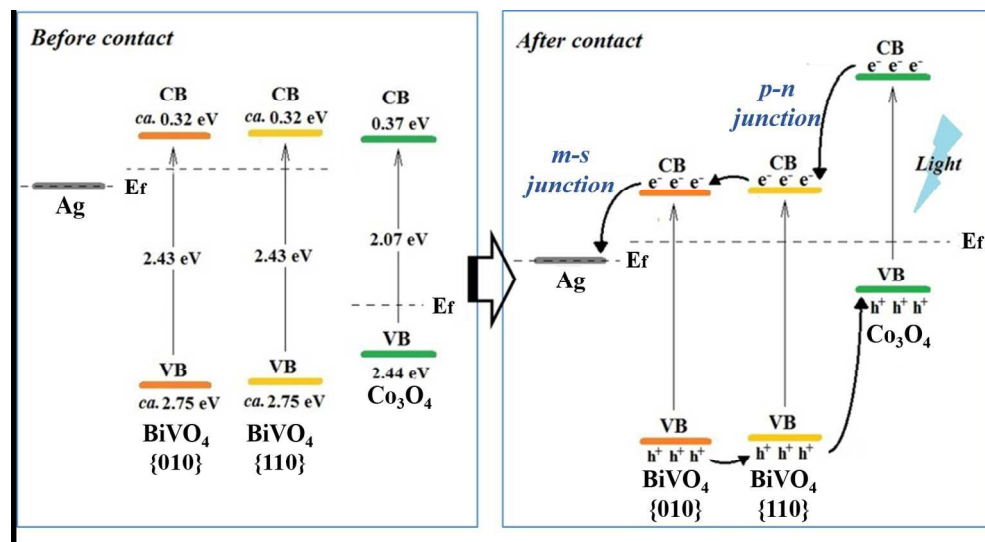
146x111mm (150 x 150 DPI)



146x110mm (150 x 150 DPI)

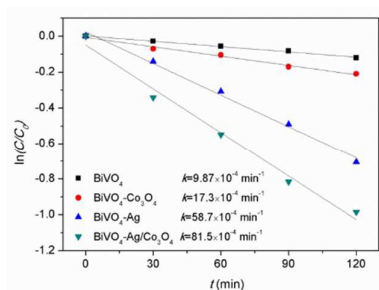


104x72mm (150 x 150 DPI)



305x164mm (150 x 150 DPI)

TOC:



The combination of p-n and m-s junctions over BiVO₄ results in an additional effect for improving photo-activity